Chapter 1
State of the Art of Metal Matrix Nanocomposites

Abstract In this chapter, the state of art of metal matrix nanocomposites (MMnCs) is discussed. In particular, the sintering methods used so far by researchers to prepare different combinations of metal matrix and nanoparticles as well as the possible applications of nanocomposites are described. The strengthening mechanisms involved in the extraordinary mechanical properties of MMnCs are also introduced, reporting the literature formulas used to calculate their contributions to the final strength of the material. In this work, Al-based composites reinforced with nanoparticles were prepared via powder metallurgy methods, first by grinding different mixtures of powders via high-energy ball milling, then by compacting powders through equal channel angular pressing (ECAP) and hot extrusion. Therefore, these processing techniques are thoroughly described in this introductory study.

Keywords Metal matrix nanocomposites · Strengthening mechanisms · Reinforcement · Ball milling · Powder metallurgy · ECAP · Extrusion

1.1 Metal Matrix Nanocomposites

Metal matrix nanocomposites are a new class of materials consisting of two or more physically and/or chemically distinct phases [1, 2]. The composites generally own some superior characteristics than those of each of the individual components. A number of processing routes are available for the synthesis of nano-reinforced metal matrix composites. They are based either on solid sintering or on liquid processing. Consolidation of powder, generally preceded by high-energy ball milling, can be carried out both by conventional technique (hot isostatic pressing, forging or cold isostatic pressing followed by heat treatment) or by alternative methods, such as ECAP or hot extrusion. Among the liquid processes, promising results were achieved by ultrasonic assisted casting. MMnCs are very interesting materials with high potential for use in a large number of industrial applications. Some recent research works highlighted the real possibility to produce composites

R. Casati, *Aluminum Matrix Composites Reinforced with Alumina Nanoparticles*,
PoliMI SpringerBriefs, DOI 10.1007/978-3-319-27732-5_1

characterized by exciting mechanical properties, which can be further enhanced by optimizing the particle dispersion. In particular, remarkable results in terms of hardness, mechanical strength, wear resistance, creep behavior and damping properties were achieved in several pioneering research works [1, 2]. By the adoption of this class of composites, expensive heat treatment (typically solution annealing and precipitation aging) currently carried out on conventional monolithic alloys could be avoided and the range of available alloys for structural and functional applications could be broadened. Notwithstanding their potential properties, there are still some aspects to be improved in production of metal matrix composites (MMCs) reinforced with nanoparticles. Their fabrication is much more complicated than that of conventional composites reinforced with fibers or micro-reinforcements. When the particles scale down from the micro- to the nano-level, many additional difficulties have to be solved and new issues have to be faced. The reaction between ceramic nanoparticles or carbon nanotubes with the matrix is still unclear. The inappropriate bonding interface may lead to the failure of the composites. Clustering of particles is another issue of paramount importance to be solved, especially for the production of large parts [1, 2].

1.1.1 Type of Metal Matrices and Reinforcements

Several metallic materials have been considered as matrix constituent for the preparation of MMnCs. In particular, the most interesting metals for industrial applications are Al [3–28], Mg [29–37], Ti [38–40], Cu [41–44] and their alloys. Pure and alloyed aluminum is among the most investigated materials with the largest number of published research studies describing Al-based composites as possible candidates for structural applications. Different species of nano-sized oxides (Al_2O_3, Y_2O_3) [8, 15, 21–23, 43, 45], nitrides (Si_3N_4, AlN) [34], carbides (TiC, SiC) [4, 13, 16, 18, 24, 25, 28, 30–33], hydrides (TiH_2) [36] and borides (TiB_2) [17, 42] have been employed as reinforcement agents. Moreover, different allotropes of carbon (carbon black [7], fullerenes [37] and carbon nanotubes (CNTs) [3, 19, 20, 35, 41, 44, 46]) have been investigated as fillers for several research works published in literature. The most used particles are CNTs: if well dispersed they are able to confer very high mechanical properties to the metal matrix and can lead to increased electrical conductivity, which makes MMnCs very attractive materials for electrical and electronic applications. Single wall carbon nanotubes (SWCNT) and multi-wall carbon nanotubes (MWCNT) have been both used for MMnCs production. In this regard, for example copper-0.1 wt% MWCNT composites revealed a 47 % increase in hardness and bronze-0.1 wt% SWCNT showed a 20 % improved electrical conductivity [41]. Finally, intermetallic compounds (NiAl, Al3Ti) had also been successfully used as reinforcement phase in MMnCs [14, 47]. Al-Al3Ti nanocomposite revealed good mechanical behavior at high temperature [47], while TiAl-NiAl MMnCs showed low fracture toughness and very high hardness [14].

1.1.2 Strengthening Mechanisms

The high strength of metal matrix nanocomposites is the result of several strengthening mechanism contributions, namely:

i. load-transfer effect (or load-bearing effect), which is due to the transfer of load from the metal matrix to the hard reinforcement [4];
ii. Hall-Petch strengthening (or grain boundaries strengthening), which is related to the grain size of the metal matrix. Nanoparticles may play a fundamental role in matrix grain refinement [48–50];
iii. coefficient of thermal expansion (CTE) and elastic modulus (EM) mismatch, which are responsible of creating dislocation networks around the particles [51, 52].
iv. Orowan strengthening, due to the capability of nanoparticles to obstacle the dislocation movement [50, 53, 54];

Moreover, like any other metallic material, the MMnCs can be further strengthen by Hull and Bacon [50]:

v. work hardening (or strain hardening or cold working), i.e. plastic deformation of metal, which leads to dislocation multiplication and development of dislocation substructures;
vi. solid-solution hardening, which can be obtained by adding interstitial or substitutional atoms in the crystal lattice which are responsible for the deformation of the lattice itself and for the formation of internal stresses;
vii. precipitation hardening (or age hardening), which relies on changes in solid solubility with temperature, to produce fine precipitates which impede the movement of dislocations, or defects in a crystal lattice. Dislocations can cross the particles by cutting them or they can bow around them by the Orowan mechanism.

Thus, several concurrent effects contribute to the final strength of MMnCs. The strengthening effects are superimposed and connected to each other; therefore, it is not yet clear how to attribute to the single effects the right contribution (weight) to the final strength. Nevertheless, several methods to predict the final strength of the nanocomposites were proposed in the open literature.

In the following sections, the strengthening methods correlated to the addition of nanoparticles in the metal matrix (i.e. points of the list from i to iv), as well as the models for estimating the final strength of the nanocomposites are described.

1.1.2.1 Load Transfer Effect

The transfer of load from the soft and compliant matrix to the stiff and hard particles under an applied external load, contributes to the strengthening of the base material. A modified Shear Lag model proposed by Nardone and Prewo [4] is commonly

used to predict the contribution in strengthening due to load transfer in particulate-reinforced composites [52–54]:

$$\Delta\sigma_{LT} = v_p\sigma_m\left[\frac{(l+t)A}{4l}\right] \tag{1.1}$$

where v_p is the volume fraction of the particles, σ_m is the yield strength of the unreinforced matrix, l and t are the size of the particulate parallel and perpendicular to the loading direction, respectively. For the case of equiaxed particles [52], Eq. (1.1) reduces to:

$$\Delta\sigma_{LT} = \frac{1}{2}v_p\sigma_m. \tag{1.2}$$

1.1.2.2 Hall-Petch Strengthening

The grain size has a strong influence on metal strength since the grain boundaries (GBs) can hinder the dislocation movement. This is due to the different crystal orientation of adjacent grains and to the high lattice disorder characteristic of these regions, which prevent the dislocations from moving in a continuous slip plane. Impeding dislocation movement, GBs hinder the extensive onset of plasticity and hence increase the yield strength of the material. When an external load generates a shear stress in a material, existing dislocations and new dislocations move across the crystalline lattice until facing a GB, which creates a repulsive stress field to oppose the dislocation movement. Then, dislocation pile up occurs generating extensive repulsive stress fields that act as a driving force to reduce the energetic barrier for their diffusion through the boundary. A decrease in grain size leads to a decrease in the amount of extensive pile ups (Fig. 1.1). Then the necessary load to be applied for dislocation movement through the material must be higher. The higher the applied stress needed to move the dislocations, the higher the yield strength [48, 49].

The Hall-Petch equation relates the strength with the average grain size (d) [38, 48, 49]:

$$\Delta\sigma_{\mathrm{H-P}} = \frac{\mathrm{k_y}}{\sqrt{\mathrm{d}}} \tag{1.3}$$

where $\mathrm{k_y}$ is the strengthening coefficient (characteristic constant of each material). The particles play a fundamental role in final grain size found in metal matrices of composites since they can interact with grain boundaries acting as pinning points, retarding or stopping their growth on high-temperature processing. The increase of v_p (volume fraction) and the decrease of d_p (particle diameter) lead to a finer structure, as theoretically modeled by the Zener equation [52]:

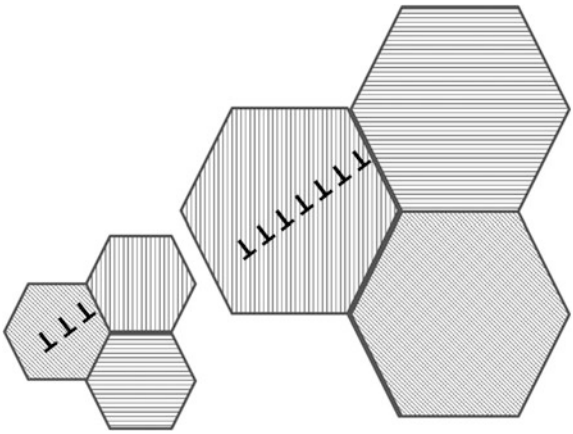

Fig. 1.1 Schematic of the Hall-Petch strengthening mechanism. Dislocations are sketched using the reversed symbol "T"

$$d_m = \frac{4\alpha d_p}{3v_p} \tag{1.4}$$

where α is a proportional constant.

There is a limit to this strengthening mechanism. For grain sizes lower than a threshold value d^* [55–66], the size of dislocations begins to approach the size of the grains, prohibiting dislocation wide-ranging pile-ups and instead resulting in grain boundary sliding or rotating, resulting in a decrease in the material's yield strength and an in increase in ductility (superplasticity). Therefore, the mechanical behavior of nanocrystalline materials is said to deviate from the classical Hall-Petch relation, below which the k value gradually decreases as the grain size is reduced (i.e. less effective strengthening). Eventually, nanocrystalline materials may soften, as the grain size is further reduced, and this effect is termed the inverse Hall-Petch relationship (often observed in metals having a crystallite size of a few units of nanometer).

1.1.2.3 Orowan Strengthening

The so-called Orowan mechanism consists in the direct interaction of nano-particles with dislocations. The non-shearable ceramic particles pin the crossing dislocations and promote dislocation bowing around the particles (Orowan loops) under external load (Fig. 1.2) [50].

The Orowan effect can be evaluated by the following expression:

$$\Delta\sigma_{OR} = \frac{0.13bG}{d_p\left(\sqrt[3]{\frac{1}{2}v_p} - 1\right)} \ln\left(\frac{d_p}{2b}\right) \tag{1.5}$$

where b is the Burger's vector and G is the matrix shear modulus.

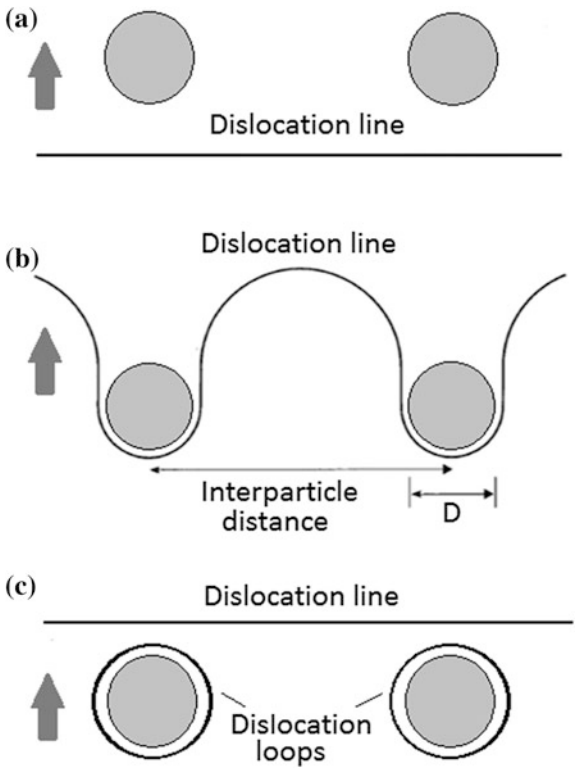

Fig. 1.2 Schematic of the Orowan strengthening mechanism [50]

Orowan strengthening is more relevant to MMnCs with particle sizes smaller than 100 nm [52–54, 67, 68]. This is because larger sized particles lead to large interparticle distance for the same volume fraction of particles and tend to segregate to the GBs. Under these circumstances, the contribution of Orowan bowing mechanism becomes negligible.

1.1.2.4 CTE and EM Mismatch

Even after perfectly matching processing conditions (amount of given deformation, times and temperatures of processing and heat treating) much higher dislocation density exists in the matrix of a composite than in the unreinforced matrix due to thermal residual stresses. The increase in dislocation density from the contribution of residual plastic strain develop during post processing cooling as a result of different coefficient of thermal expansion (CTE) between the matrix and reinforcing phase. The high stress field around the reinforcement is relaxed by the generation of dislocations at the matrix-reinforcement interface. Such dislocations are also called geometrically necessary dislocations (GNDs). Also the gap in elastic modulus

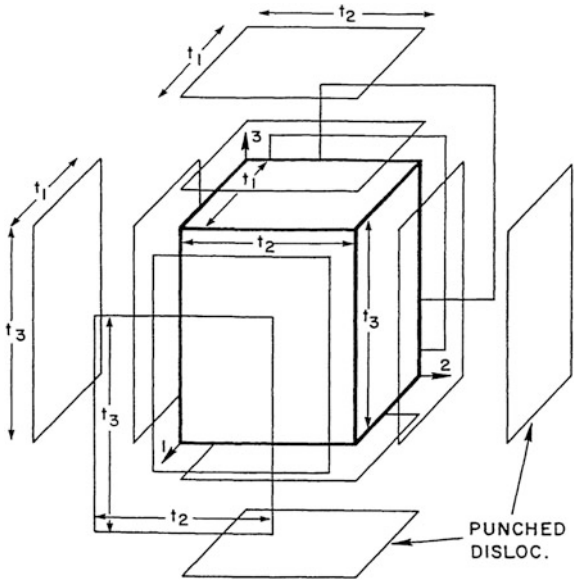

Fig. 1.3 Schematic of the model for "punching" of prismatic dislocation loops to relax the CTE misfit at the matrix/particulate interface [70]

(E) between the stiff particles and the compliant matrix can lead to the formation of additional dislocations during the elastic straining of the nanocomposites. GND density due to CTE (ρ^{CTE}) and Young modulus (ρ^{EM}) mismatch can be estimated by the following expressions [51, 52, 69, 70]:

$$\rho^{CTE} = \frac{A\Delta\alpha\Delta T v_p}{bd_p(1-v_p)} \tag{1.6}$$

$$\rho^{EM} = \frac{6v_p}{\pi d_p^3}\varepsilon \tag{1.7}$$

where A is a geometric constant, $\Delta\alpha$ is the difference in CTE and ΔT is the difference between test and processing or heat treatment temperatures. Arsenault and Shi [70] firstly proposed Eq. 1.6, which was supported by the so called "dislocation punching model" (Fig. 1.3). The combined strengthening due to CTE and E GNDs can be calculated by means of the Taylor equation [71]:

$$\Delta\sigma_{CTE+EM} = \sqrt{3}\beta Gb\left(\sqrt{\rho^{CTE}} + \sqrt{\rho^{EM}}\right) \tag{1.8}$$

where β is a constant.

1.1.2.5 Sum of Contributions

The final strength of the MMnC is quite difficult to be estimated; to this purpose, different models have been proposed. The easiest one does not take into account the overlapping of the concurrent strengthening effects [52]. It evaluates the final strength of the composite, σ_c, by simply summing the contributions related to the single strengthening effects, $\Delta\sigma_i$, with the original yield strength of the unreinforced matrix, σ_m, therefore:

$$\sigma_c = \sigma_m + \sum_i \Delta\sigma_i \tag{1.9}$$

Other studies proposed alternative methods to calculate σ_c, considering the superposition of the effects. A simple model [51, 52], which approaches quite well the experimental data, suggests to calculate the final strength of the composite by summing the root of the squares of all the single strengthening contributions, as:

$$\sigma_c = \sigma_m + \sqrt{\sum_i \Delta\sigma_i^2} \tag{1.10}$$

Another common method that takes into account Orowan strengthening effect, dislocation density due to the residual plastic strain caused by the CTE mismatch and load-bearing effect was proposed by Zhang and Chen [53, 54]:

$$\sigma_c = (1 + 0.5v_p)(\sigma_m + A + B + \frac{AB}{\sigma_m}) \tag{1.11}$$

where A is the term relative to CTE mismatch and B is the coefficient related to Orowan effect:

$$A = 1.25 G_m b \sqrt{\frac{12\Delta\alpha\Delta T v_p}{b d_p (1 - v_p)}} \tag{1.12}$$

$$B = \frac{0.13 G_m b}{d_p \left[\left(\frac{1}{2v_p} \right)^{\frac{1}{3}} - 1 \right]} \ln \frac{d_p}{2b} \tag{1.13}$$

Few papers are available in literature about this topic. This lack does not allow a comprehensive evaluation and comparison of the proposed methods based on a physics ground.

1.1.3 Preparation Methods and Properties

For the large-scale production of metal matrix nanocomposites, the main problem to face is the low wettability of ceramic nano-particles, which does not allow the preparation of MMnCs by conventional casting and melting processes since the result would be an inhomogeneous distribution of particles within the matrix. The high surface energy (related to very high surface-to-volume ratio) readily leads to the formation of clusters of nanoparticles, which are not effective in hindering the movement of dislocations and can hardly generate a physical-chemical bond to the matrix, thus reducing significantly the strengthening capability of nanoparticles [1, 46]. Several unconventional production methods have been studied by researchers in order to overcome the wettability issue, either by formation of the reinforcement by in situ reactions or by ex situ addition of the ceramic reinforcement by specific techniques. Hereafter, the most studied and successful methods are described by classifying them into liquid, semisolid and solid processes.

1.1.3.1 Liquid Processes

For composites prepared by the conventional liquid metallurgy route, severe aggregation of nanoparticles frequently occurs even when mechanical stirring is applied on the melt before casting. This is due to poor wettability and high viscosity generated in the molten metal owing to high surface-to-volume ratio of the nano-sized ceramic particles. The density of nanoparticles do not play an important role in the production process of nanocomposites. Such small particles are supposed to float on the top of the molten bath even if their density is relatively higher than that of the liquid matrix. This mass-mismatch issue was indeed very significant in micron-sized particle reinforced composites but in nano-reinforced materials, other effects such as those induced by extensive surface tension play a much more important role [72].

High-intensity ultrasonic waves revealed to be useful in this context since they produce acoustic transient cavitation effects, which lead to collapsing of micro-bubbles. The transient cavitation would thus produce an implosive impact, strong enough to break the nanoparticle clusters and to uniformly disperse them in the liquid metal. According to this technique, a good dispersion of 2 % of SiC nano-particles in aluminum alloy 356 was achieved by Li et al. [13] by means of the experimental setup equipped by ultrasonic source. An improvement of 20 % in hardness over the unreinforced alloy was achieved. Lan et al. produced nano-sized SiC/AZ91D Mg alloy composites through the same method (see the experimental device in Fig. 1.4). A fairly good dispersion of the particles was achieved although some small clusters still occurred into the matrix. Owing to general improvement of the dispersion, the 5 wt% SiC reinforced composite led to a microhardness increase of 75 % [73]. As already mentioned, the nanoparticles also play a fundamental role in grain refinement, working as pinning points, hampering the grain growth and leading to improved mechanical properties according to Eqs. (1.3) and (1.4).

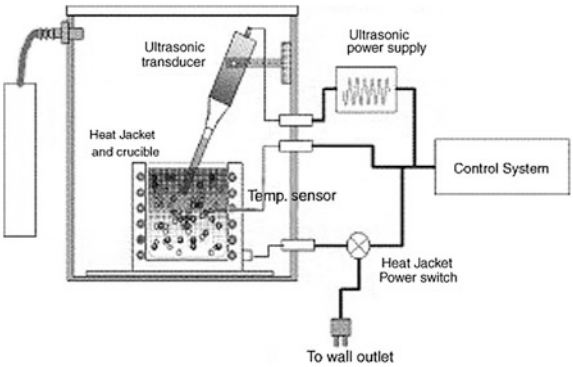

Fig. 1.4 Schematic of the experimental setup used by Lan et al. [73] for ultrasonic dispersion of nanoparticles

In this regard, it has been reported that an addition of 1 wt% nano-SiC into pure Mg strongly acts in this direction. Under comparative processing conditions, the Mg/SiC composite featured an average grain size of 72 μm whereas the unreinforced pure Mg showed an average size of 181 μm [30]. Moreover, De Cicco and co-workers [27, 28] proved by a droplet emulsion technique (DET) that nanoparticles can catalyze nucleation, thereby reducing undercooling. For A356 alloy based nano-composites produced by ultrasonic assisted casting, γ-Al_2O_3 revealed a better nucleation catalyzer than α-Al_2O_3 probably due to its lower lattice mismatch with the metal matrix. Other tests were also conducted in the same research [28] with TiC and SiC of different sizes.

Tensile tests performed on AZ91D alloy and on the same material reinforced by 1 wt% of nano-AlN produced by ultrasound-assisted casting revealed an increase of yield strength in MMnCs of 44 % at room temperature (RT) and of 21 % at 200 °C when compared to the unreinforced AZ91D alloy. For the same materials, a decrease of fracture strain at room temperature (RT) was achieved while an enhanced ductility was measured at 200 °C [34]. Improved ductility was also detected by Wang et al. [31] even at RT. The yield strength (YS), ultimate tensile strength (UTS) and fracture elongation of an AZ91 alloy were 104, 174 MPa and 3.6 %, respectively whereas the corresponding values for the AZ91 alloy reinforced by 0.5 wt% of 50 nm SiC were: 124, 216 MPa and 6.6 %, respectively. In a research work by Cao et al. [74], the addition of 1.5 wt% SiC to Mg-4Zn alloy obtained by an ultrasonic cavitation-based solidification process led to an increase of RT ductility of more than twice as well as to improved YS and UTS. The same authors also observed a reduction of grain size in reinforced sample (150 μm vs. 60 μm) which was also related to improved castability of the alloy.

Disintegrated melt deposition (DMD) is a further liquid metallurgy process successfully employed for nano-composite production (Fig. 1.5). Alumina nanoparticles have been well dispersed in Al–Mg alloys by heating the metal in argon atmosphere and adding the ceramic particles by means of a vibratory feeder. The melt was stirred and poured, then disintegrated with argon gas jets and deposited onto a metallic substrate. Finally, the MMnCs were extruded to reduce porosity down to very low levels and to achieve a good dispersion of the particles [75, 76].

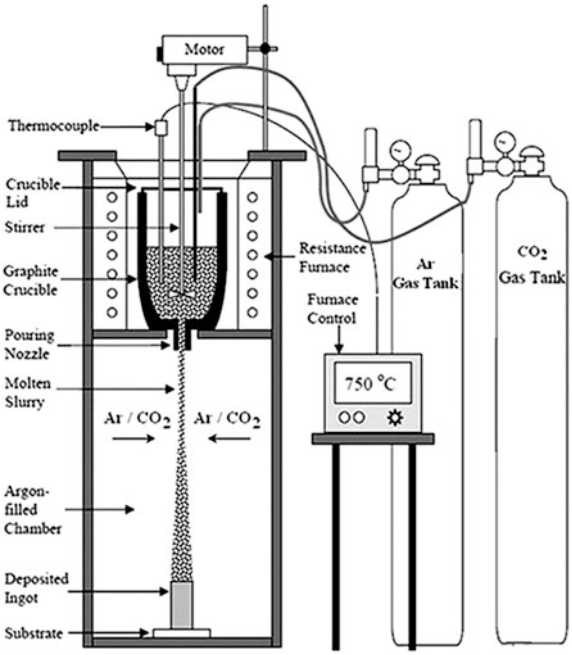

Fig. 1.5 Schematic of the experimental setup used for disintegrated melt deposition (DMD) process [75]

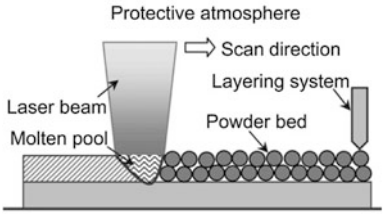

Fig. 1.6 Schematic of selective laser melting process [77]

Selective laser melting (Fig. 1.6) was also used to produce Ti-based composites reinforced by nanoparticles [77]. Powders were milled by high-energy ball milling and then melted by laser beam under protective atmosphere. Through this method, a unique material featuring a very different microstructure of the reinforcement was achieved. A proper decrease in volumetric energy density led to the development of TiC whiskers and of uniformly dispersed nano-lamellar TiC starting from dendritic TiC. The same research confirmed that well dispersed nano-particles induce improved mechanical and wear properties to the Ti matrix.

MMnCs reinforced with nanoparticle formed in situ have been successfully prepared by liquid metallurgy processes. 50 nm TiB_2-reinforced copper-matrix

composites were produced by adding B_2O_3, C and Ti in a Cu-Ti melt [78]. The composites exhibited significantly improved mechanical properties. In particular, the YS of Cu and Cu/TiB_2 was 298.7 and 509.6 MPa, respectively. Al/TiB_2 nanocomposites were also synthesized by an in situ method, by adding a mixture of potassium hexafluorotitanate (K_2TiF_6) and potassium tetrafluoroborate (KBF_4) salts in an Al melt under argon atmosphere [79].

High-pressure die casting [35] and arc-discharge plasma method [80] were also used to produce AZ91/CNT composites and in situ Al/AlN MMnCs, respectively.

Finally, it was highlighted that the main problem to be faced in production of CNT-MMnCs by the liquid metallurgy method is the interaction of the nanotubes with the liquid metal. In fact, the process may cause damage to CNTs or formation of chemical reaction products at the CNT/metal interface [46, 81, 82]. Therefore, this synthesis route is mainly indicated for those composite matrices having low-melting temperatures and reduced reactivity with the reinforcement phases. The problem of low wettability of CNTs can be partially overcome by coating CNT with metal layers (for example Ni) [46, 83]. The field of surface modification appears as quite promising and it is open to innovation for attenuating the drawbacks about wettability and tendency to clustering of nanoparticles.

1.1.3.2 Semi-Solid Processes

Only few works are available in literature about this topic even if this method has been widely applied for micrometer-size particle-reinforced MMCs, and it would be extremely interesting for large-scale production.

A356/Al_2O_3 MMnCs were produced by using a combination of rheocasting and squeeze casting techniques [84]. Rheocasting is a semi-solid phase process, which has several advantages: it is performed at lower temperatures than those conventionally employed in foundry practice resulting in reduced thermochemical degradation of the reinforcement surface. Moreover, the material shows thixotropic behavior typical of stir cast alloys and production can be performed by conventional foundry methods. During rheocasting, the pre-heated nanoparticles are added in the semi-solid slurry while it is vigorously agitated in order to achieve a homogenous particle distribution. Then the slurry is squeezed using a hydraulic press. Mg alloy AZ91 ingots reinforced by nano-SiC particles were produced by semisolid stirring-assisted ultrasonic vibration [33]. After homogenization treatment and extrusion, the SiC reinforcement featured a fairly good dispersion although bands of accumulated nanoparticles were present and their amount could be reduced by increasing the extrusion temperature.

An innovative method named semi-solid casting (SSC) was proposed by De Cicco et al. (Fig. 1.7) [85]. Zinc alloy AC43A reinforced by 30 nm β-SiC was used for sample preparation by SSC. The SSC experiments were carried out by pouring ultrasonicated molten MMNC material (450 °C) from a graphite crucible into a steel injection device, which was preheated to 400 °C. Liquid MMnC was cooled down to 386 °C achieving less than 30 % of solid fraction. Then, the injection sleeve was

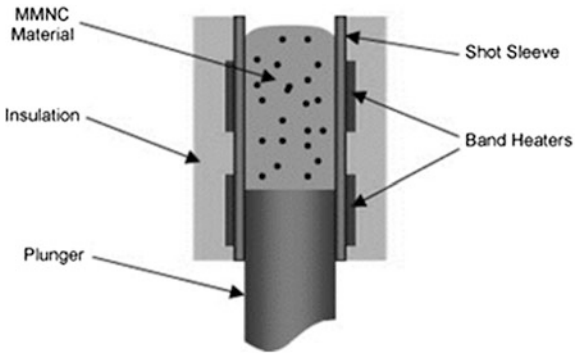

Fig. 1.7 Schematic of experimental setup of the semi-solid casting (SSC), which was proposed by De Cicco et al. in [85]

inverted and placed on top of a steel mold. The plunger was activated and the semi-solid material was injected into the mold. The produced samples showed strength properties comparable to those produced by ultrasound-assisted casting but with improved ductility due to the nucleation catalysis by the β-SiC nanoparticles that refines the microstructure of the MMnC.

1.1.3.3 Solid Processes (Powder Metallurgy)

Several solid methods were studied and developed for preparing MMnCs. In particular, different powder metallurgy techniques were successfully employed in this respect. Some papers focus on mechanical alloying which is a powder metallurgy technique consisting in repeated cold welding, fracturing and re-welding of powder particles in a high-energy ball mill. This technique is of fundamental importance since it allows achieving a better dispersion of nano-powder into the composite by breaking up the ceramic clusters. It can also be exploited for the formation of alloys by diffusion mechanisms starting from pure metals, and to produce preforms by in situ reaction of nano-reinforcements. Therefore, mechanical alloying, which cannot be separated from the opportunity of breaking up the nano-ceramic clusters, is a value-added option offered by this particular processing route [22, 24, 28, 36, 42, 86–95]. It has been proved that the presence of nanoparticles can accelerate the milling process (stimulating plastic deformation, cold welding, and particle fragmentation) and grain refinement mechanism [89–91]. Process control agent (PCA) has a strong influence on morphological evolution of powders during ball milling [23]. The addition of 1.5 % stearic acid as PCA prevents extensive cold welding of Al particles during ball milling and leads to an increase of hardness of the hot-compacted samples. Speed and time of milling, mass of balls and powder, ball diameter also contribute to final hardness development. In particular, a pronounced decrease in energy transfer from the balls to the powder was found by raising the amount of balls [24].

High-energy ball milling proved to be a suitable technique for the production of in situ MMnCs. Al-TiN composite was prepared by milling elemental Al and Ti

powders with ring-type organic compound pyrazine in benzene solution [87]. Mg 5 wt% Al alloy in situ reinforced with TiH_2 was also prepared by mechanical alloying of elemental powder of Mg, Al and Ti, using polyethylene-glycol to provide hydrogen for the formation of TiH_2 and to prevent excessive cold welding during ball milling. After attritioning, the powders were cold isostatically pressed (CIP), extruded and thermal treated. The mechano-chemically milled specimens showed very fine microstructure and good dispersion of fine reinforcements, a slight increase in YS and ductility was observed [36, 92]. Iron-wustite (Fe–FeO) nanocomposites were also produced by mechano-chemical processing starting from Fe and Fe_2O_3 powder with different mole ratios. These materials showed a ferromagnetic-like behavior, which was interpreted according to spinel-like defect, clusters [88]. Mg-5%Al-10.3%Ti-4.7%B (wt.) powders were ground using high-energy ball milling and extruded by Lu et al. They observed the formation of non-equilibrium Ti_3B_4 phase in extruded samples [90]. Lu and co-authors investigated the in situ formation of TiB_2 via chemical reaction among Al, TiO_2 and B_2O_3. The powders were cold compacted into green compacts and sintered at different temperatures. By this method, 53 % improvement in both YS and UTS was achieved [17]. In situ TiB_2 reinforced Cu alloy composite was indeed achieved via argon atomization at 1400 °C followed by hot isostatic pressing (HIP) at 200 °C under 200 MPa pressure [42]. Moreover, Cu-Al_2O_3 nanocomposites have been prepared by two chemical routes: through decomposition of $Al(NO_3)_3$ to Al_2O_3 by calcination of a paste of CuO-$Al(NO_3)_3$ followed by H_2 reduction and sintering, or through hydrolysis of $Al(NO_3)_3$ solution followed by calcination, reduction and sintering. The latter method led to the formation of finer Al_2O_3 (30 nm vs. 50 nm) nanoparticles and promoted enhanced properties in terms of relative density, microhardness and abrasive wear resistance [86]. Submicron-sized titanium carbide was successfully sintered from the reaction of Ti salt (K_2TiF_6) and activated carbon, by controlling the degree of reaction through temperature and amount of C. In this respect, it was observed that at low temperatures, formation of Al_3Ti was predominant while at high temperatures (above 1000 °C), the intermetallic compound was not stable and TiC was preferentially formed [25].

Several techniques have been used to perform the compaction of composite powders. The most common routes are HIP [42], hot pressing [43] and cold pressing [15, 17, 45, 93–95] or CIP [36, 92] followed by a sintering treatment. Conventional hot extrusion [19, 32, 96, 97] or equal channel angular extrusion (ECAE), also known as equal channel angular pressing (ECAP) [7, 8, 10, 21, 23, 26, 44, 98–100] revealed to be suitable methods to achieve full dense composites. Hot extrusion was used to sinter Al-2 % CNT composite powders blended by high-energy ball milling, observing a tensile strength enhancement of 21 %. Extrusion was also found to promote alignment of CNTs along the extrusion direction that may lead to anisotropic properties of the material [19]. In the same work, CNTs have been found to act as nucleation sites for void formation during tensile tests. Both CNTs pullout and MW-CNT inner tubes slippage were observed in fractured surfaces, suggesting poor interfacial bond between CNTs and Al matrix. Ferkel et al. extruded at 350 °C pure Mg powders and two composite

powders consisting of Mg and 3 wt% nano-SiC. One batch had been ball milled and the second one had been conventionally mixed [32]. The study was focused on high temperature mechanical behavior of the produced nanocomposites. The milled composite showed the largest gain in strength but also the lowest ductility at all testing temperatures (RT, 100, 200 and 300 °C). Moreover, significant difference in the creep response was been observed at 200 °C in favor of the ball-milled composite. Al-based samples sintered by ECAP and sintered by cold pressing followed by heat treatment and extrusion were compared in [21]. The best results were achieved by the former method since the hardness values after three ECAP passes was 67 % higher than the extruded samples. Higher compressive strength and increased wear resistance were also achieved in the ECAP processed samples. ECAP powder pressing was successfully used to consolidate 1 % CNTs in copper matrix at room temperature, avoiding CNT surface reaction with metal matrix [44]. Al nanocomposites reinforced by carbon black (CB) or by Al_2O_3 were also produced by using back-pressure ECAP at 400 °C [7, 8, 10]. In particular, good dispersion of Al_2O_3 and CB nanoparticles was achieved by mechanical milling followed by 8 ECAP passes. Compression tests performed on these materials showed that the YS of unreinforced sample reached 58 MPa, while that of the composite with addiction of 5 % CB reached 260 MPa. Moreover, after 8 ECAP passes, fully dense pure Al showed a Vickers hardness of 37.1 HV, while the Al-5 % Al_2O_3 MMnC showed an hardness of 96.5 HV and the Al-5 % CB system an hardness of 81 HV [7, 10]. Al composites reinforced by 5, 10 and 15 % nano-Al_2O_3 were also produced by powder metallurgy route. The powders were mixed in ethanol by ultrasonic treatment, wet attritioned by high-energy ball milling and finally compacted by ECAP at 200 °C. The best results in terms of microhardness and compressive yield stress were achieved by adding 10 % nano-alumina after 4 ECAP passes [26]. Milling associated to ECAP process of chips revealed to be a further promising route for the use of metal scraps [38, 99]. Ceramic nanoparticles (AlN) were successfully added to Mg-5 % Al alloy chips even though no significant improvement in strength could be achieved [98].

Since in this work MMnCs have been produced via powder metallurgy route, first by grinding the powders by high-energy ball milling, then by compacting them via ECAP or hot extrusion, in the next sections these processes will be thoroughly debated.

1.2 Processing of Metal Powders

There are several methods employed for processing and consolidating metal powders. Most of the consolidation methods are based on the sintering process, which relies on diffusion of atoms between powder particles at fairly high temperatures. Other methods are indeed based on plastic deformation of metal powders. Hereafter, high-energy ball milling, which is a technique for grinding and

modifying powders, and ECAP and extrusion, which are process used for consolidation of powders, are described in details being of particular interest for this work.

1.2.1 High-Energy Ball-Milling

Mechanical alloying is a powder processing technique that allows the production of homogeneous materials starting from blended elemental powder mixtures. It was firstly developed by John Benjamin in 1966 [101]. A popular technique to perform mechanical alloying is the high-energy ball milling (BM). It consists in vials filled with powders and grinding balls, which can rotate with planet-like motion at very high speed. BM produces nanostructured particles through structural decomposition/refinement of initially coarse grained structures by severe plastic deformation (SPD) [101, 102]. Minimum grain sizes measuring few tens of nanometers can be easily obtained in ball milled powder particles. Moreover, BM is a versatile powder processing technique that is capable of producing powder with unique and far-off equilibrium microstructures. During high-energy milling, the powder particles are repeatedly attritioned, cold welded, fractured and rewelded. The force of the impact plastically deforms the powder particles trapped within two colliding balls, leading to extensive work hardening and fracture. The new fresh surfaces enable the particles to weld together leading to an increase in particle size. In a second stage of the process, the particles get work hardened and fatigue fractures may occur. At this stage, the tendency to fracture predominates over cold welding. After milling for a certain time, equilibrium is established between the welding and the fracturing rates. Smaller particles are able to withstand deformation without fracturing and tend to be welded into larger clusters, with an overall tendency to drive both very small and very large particles towards an intermediate size [101].

It is clear that during mechanical alloying, severe deformation is introduced into the powder particles. This is readily proven by the high amount of crystal defects, such as dislocations, vacancies, stacking faults, and grain boundaries. The presence of this defects also increase the diffusivity of solute elements into the matrix. Moreover, the rise in temperature during milling, which can be controlled by milling parameters, further helps the diffusion processes, and consequently promotes effective alloying amongst the constituent elements [101, 103, 104]. It is possible to conduct mechanical alloying of three different combinations of materials:

- Ductile-ductile system. The condition for alloying to take place during BM is fracturing and cold-welding of the mixture to introduce crystal defects such as dislocations, vacancies, stacking faults, and grain boundaries. This leads to enhanced diffusion of solute elements into the matrix and decreased diffusion distances. Thus, the ductile-ductile system is the easiest combination to achieve by mechanical alloying since cold welding cannot take place if the particles are too brittle [101, 103, 105].

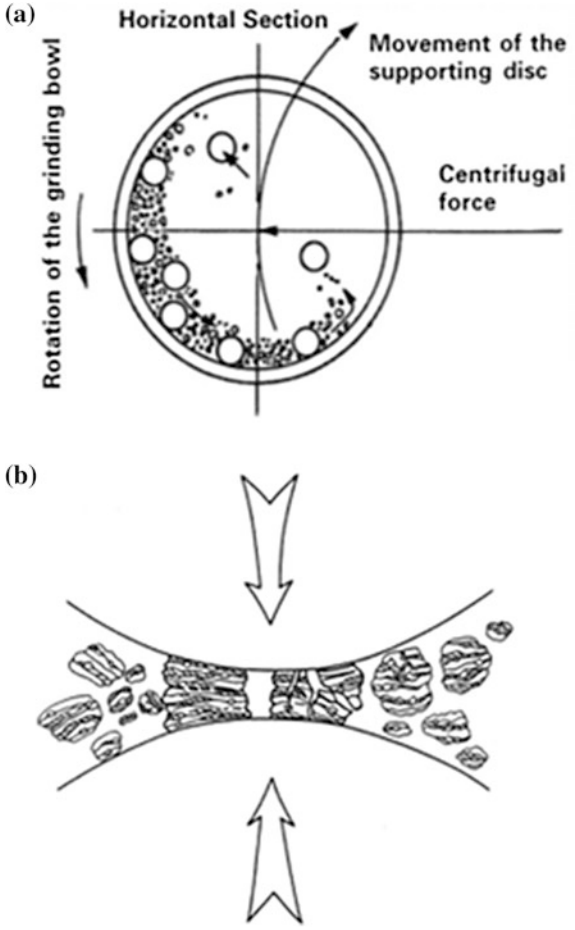

Fig. 1.8 Schematics depicting **a** the ball motion inside the mill and **b** the collision ball-powder-ball during mechanical alloying [101]

- Ductile-brittle system. Ceramic and intermetallic particles are generally brittle. Fracture into smaller fragments occurs during early stages of BM [101, 106, 107], as illustrated in Fig. 1.8. The fragmented brittle particles tend to be enveloped by the ductile particles and are trapped at the inter-lamellar interfaces, as shown in Fig. 1.9a. Further milling convolutes and refines the ductile particles (Fig. 1.9b and c). The interlamellar spacing decreases and the brittle particles are dispersed more homogeneously. Alloying between the ductile and brittle phase may occur depending on the solid solubility of the system.
- Brittle-brittle systems. Alloying is less likely to occur during BM of brittle-brittle powder mixtures due to lack of welding. On the contrary, BM has a strong influence in powder particles size owing to marked fragmentation effects [101].

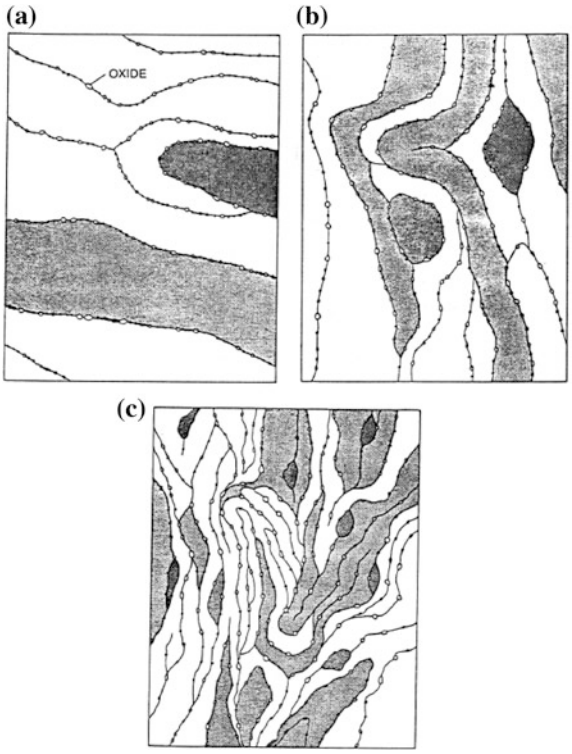

Fig. 1.9 Structural evolution of ductile-brittle system during BM for oxide dispersion strengthening alloys [101]

1.2.1.1 High-Energy Ball Milling Variables

A number of variables must be optimized to achieve the desired product phase and/or microstructure. Hereunder the most important are listed:

- Material of the vials. The material used for the milling container is important since due to impact of the grinding balls on the inner walls of the vial, some material will be dislodged and incorporated into the powder. This can contaminate the powder. Hardened C-steel, tool steel, hardened chromium steel, tempered steel, stainless steel, WC-Co, are the most common types of materials used for the grinding vessels. Some specific materials are used for specialized purposes; these include copper, titanium, sintered corundum, yttria-stabilized zirconia (YSZ), partially stabilized zirconia-yttria, agate, etc. [108–114].
- Shape of the vials. The shape of the container is also important, especially the internal design of the container, but cylindrical vials are generally employed.
- Milling speed and direction. The faster the rotation the higher is the kinetic energy transferred to the powder, but above a critical speed the balls are pinned to the vial inner walls and do not fall down to apply any impact force. Therefore, the maximum speed should be just below this threshold value so as to produce the maximum collision energy. At high speed, the temperature of the

vial-ball-powder system may reach a high value, which can be advantageous or disadvantageous depending on the purpose of the milling. Same or opposite direction of the main disk and of the planets can be chosen, this may lead to different collision configurations [101].

- Milling time and pauses. Milling time has a fundamental role on the characteristic of the final powder. The effect of the milling time on the average particle size was described in the previous part of the section. In order to decrease the temperature of the system, a certain number of pauses can be programmed. Milling times can become extremely long (several tenths of hours) to achieve the desired transformation of the powder.
- Material of the grinding balls. The materials used for the balls are the same of those used for the vials, because they possess the same criticality.
- Size of the grinding balls. Balls size has an influence on the milling efficiency. A large size of the grinding medium is useful since the larger weight will transfer more energy to the particles. It was also suggested that smaller balls produce intense frictional action, which promotes the amorphous phase formation. In fact, it appears that soft milling conditions (small ball sizes, lower energies, and lower ball-to-powder ratios) seem to favor the amorphization of the crystal structure or the formation of metastable phases [108, 115–118]. Also, different sizes balls can be used simultaneously. It has been reported that a combination of large and small size balls during milling minimizes the amount of cold welding and the amount of powder stuck onto the surface of the balls [119].
- Ball-to-powder weight ratio (BPR). The ratio of the weight of the balls to the powder is an important variable in the milling process. The higher the BPR, the shorter is the milling time required. At a high BPR, because of an increase in the weight proportion of the balls, the number of collisions per unit time increases and consequently more energy is transferred to the powder particles. It is also possible that due to the higher energy, more heat is generated and this could also change the constitution of the powder.
- Extent of filling the vial. It is necessary that there is enough space for the balls and the powder particles to move around freely in the container in order to have enough impact energy.
- Milling atmosphere. To avoid contamination, either argon or helium are generally used as protective gas. Nitrogen, air and hydrogen can lead to the in situ formation of nitride, oxide and hydride compounds.
- Process control agent. The severe plastic deformation of powder particles during milling leads to their cold-welding, but a good balance between cold welding and fracturing of particles is necessary to achieve alloying and/or good particles dispersion. A process control agent (PCA) (also referred to as lubricant or surfactant) is often added to the powder mixture to reduce the effect of welding and to inhibit the agglomeration. PCAs can be in the solid, liquid, or gaseous form. They are mostly organic compounds, which are able to act as surface-active agents. The lubricant adsorbed on particle surfaces obstructs the cold welding and lowers the surface tension of the powders. Several PCAs have

been employed at a content level of about 1–5 % of the total powder weight. The most used PCAs include stearic acid, hexane, methanol, and ethanol. Most of these lubricants decompose and form compounds with the powders during milling, which are incorporated as inclusions or dispersoids into the powder particles during milling. These are not necessarily harmful to the alloy system since they can contribute to dispersion strengthening of the material, resulting in increased strength and higher hardness. The hydrogen subsequently escapes as a gas or it is absorbed into the metal lattice on heating or sintering. Even though hydrogen gas primarily serves as a surfactant and does not usually participate in the alloying process, some reports indicate that hydrogen acts as a catalyst for amorphous phase formation in titanium-rich alloys [120–123].

- Temperature of milling. The temperature of milling can be varied by dripping liquid nitrogen on the milling container or by electrically heating the milling vial. It was reported that higher temperature results in lower strain in the material and hence bigger grain size [124, 125]. Moreover, milling temperature can modify the amorphization kinetics [126, 127].

1.2.2 Equal Channel Angular Pressing

ECAP is a widely researched SPD process able to induce large accumulative shear strain on a bulk or powdered material without significantly modifying the specimen geometry. The ECAP was firstly proposed by Segal in the former Soviet Union in the early 1970s [128]. During 1990s, with growing interest in ultrafine grained materials, ECAP was recognized as a capable SPD method and the research on ECAP gained momentum [129–131]. One of the main advantages of ECAP over other SPD processes is that it allows relatively large billets to be processed with homogeneous deformation throughout the sample.

Grain refinement by ECAP has been widely studied and many comprehensive reviews on the properties and structural evolution of ECAP processed materials are available [132–139]. ECAP was also used to refine the grains of MMC materials [140, 141]. The presence of the particles accelerates the hardening and grain refinement of the matrix phase compared to the unreinforced material. This was attributed to their role in retaining higher dislocation densities at the particle interface and in stimulating continuous recrystallization processes [141].

The basic setup for ECAP is depicted in Fig. 1.10 [133]. It consists of a die having two intersecting channels with equal cross section and a plunger that fits the entrance channel of the die. Two angles are characteristic of the ECAP die:

- The angle Φ, made by the intersect of the two channels
- The angle ψ, which describe the outer corner curvature where the two channels intersect.

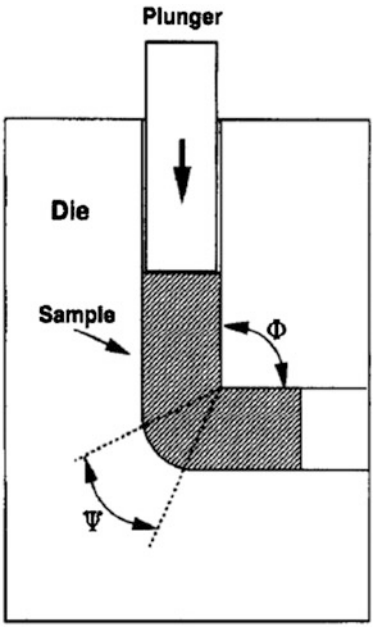

Fig. 1.10 Schematic drawing of an ECAP setup [133]

A billet, with the same cross section as the channel, is forced by a plunger to flow through the die. It is deformed by simple shear as it passes through the plastic deformation zone (PDZ) located at the intersection of the two channels.

For a round corner die, i.e. when $\psi \neq 0$, the equivalent shear strain at each pass can be calculated using the following equation [134]:

$$\varepsilon_e = \frac{1}{\sqrt{3}}\left[2\cot\left(\frac{\Phi}{2}+\frac{\psi}{2}\right)+\psi\mathrm{cosec}\left(\frac{\Phi}{2}+\frac{\psi}{2}\right)\right] \tag{1.14}$$

It is worth noting that the Eq. (1.14) is only valid under ideal conditions (i.e. simple shear). The cumulative plastic strain (or effective strain) after N number of passes can be expressed as

$$\varepsilon_{eN} = \varepsilon_{eN} * N \tag{1.15}$$

It can be easily estimated that remarkably high values of accumulated strain (of the order of several units) can be achieved by repeating more times the insertion of a billet in the ECAP die, so as to attain the expected grain refining effects.

1.2.2.1 ECAP process variables

The final characteristic of the material produced by ECAP can be tailored modifying the following process parameters:

- Geometry of the die. In particular the intersect angle Φ, and the outer angle ψ affect the equivalent strain, as previously described.
- Processing route. Different microstructures can be attained or final refinement can be achieved at different rates by simply rotating the workpiece between subsequent passes [136, 142]. Four basic processing routes are commonly employed. They are defined according to their rotating scheme around the vertical axis, namely: route A, route B_A, route B_C, and route C, as illustrated in Fig. 1.11a [142]. The different routes are able to impose different shear planes on the sample (Fig. 1.11b) [136]. It has been demonstrated that route B_C leads to the fastest transformation from subgrain boundaries to an equiaxed array of high

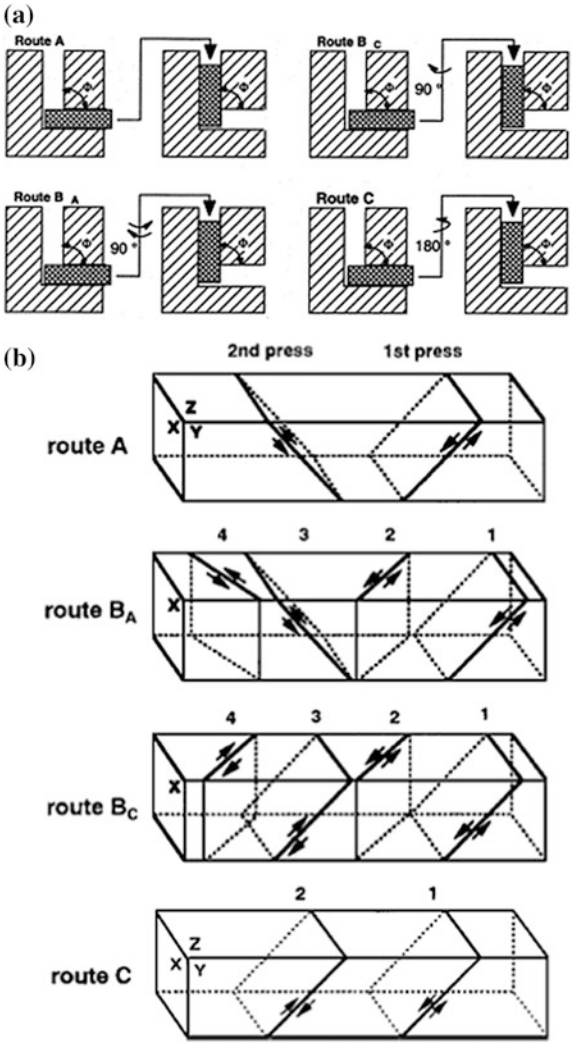

Fig. 1.11 **a** The four common processing routes used in ECAP [142]. **b** Shear planes for consecutive passes of the four fundamental ECAP routes viewed on the X, Y, and Z planes [136]

angle grain boundaries (HAGBs) by promoting the development of subgrain bands through subsequent ECAP passes on the intersecting sets of the two different shear planes [137].

- Temperature. In general, the higher the working temperature, the bigger the final grain size of the sample and the lower the achieved yield strength. Samples processed at elevated temperatures also tend to have higher fractions of low angle grain boundaries (LAGBs). During ECAP deformation, LAGBs evolve into HAGBs by absorption of moving dislocations into the boundaries. At elevated temperatures, the rate of recovery is higher and dislocations are more likely to annihilate by cross-slip rather than being absorbed into subgrain boundaries. Therefore, formation of HAGBs is reduced when the working temperature is high [143–146].
- Number of passes through the die. A minimum amount of plastic deformation (i.e.: a minimum number of passes) is required to achieve the expected microstructural evolution leading to significant grain refinement. Usually, a condition of saturation of properties is attained after a given amount of deformation which depends on nature of material, crystal structure, processing temperature and route [136, 137, 142].
- Back-pressure (BP). A constant BP can be applied on the workpiece by the use of a back-plunger [7, 147, 148]. This leads the material to be subjected to a hydrostatic pressure. BP plays only a minor role in final mechanical and microstructure properties [149]. However, it modifies the mode of deformation during ECAP closer to that of simple shear by eliminating the formation of a corner gap, improving the uniformity of the stress-strain distribution and reducing the tendency to form cracks in brittle materials [5, 150]. Applying BP implies the formation of overall more equiaxed microstructure with higher fraction of HAGBs (about +10 %) [151]. The benefits of BP are most evident when processing brittle materials which normally require high processing temperatures [152–155]: they can be processed at much lower temperatures, resulting in much finer grain structures.

1.2.2.2 Consolidation of Particles by ECAP

ECAP was first used for powder consolidation in the 1990s [156]. This technique was used to consolidate different materials starting from powders such as Al, Ti, Cu, and Mg, alloyed powders and composite powders. Traditional sintering methods are based on diffusion. Vice versa, the mechanism for ECAP consolidation is mainly by plastic deformation of the powder particles [99]. During ECAP, the particles undergo very high shear strains and plastic deformation. The high deformation breaks the brittle surface oxide films and leads to direct contact between fresh metal surfaces, and bonding between the particles can occur instantaneously (Fig. 1.12) [99].

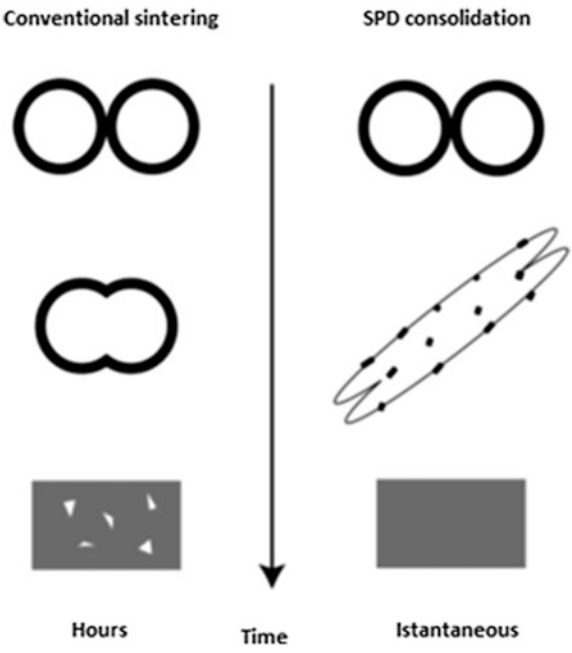

Fig. 1.12 Schematic illustration of particle consolidation in conventional sintering (*left*) and ECAP consolidation (*right*) [99]

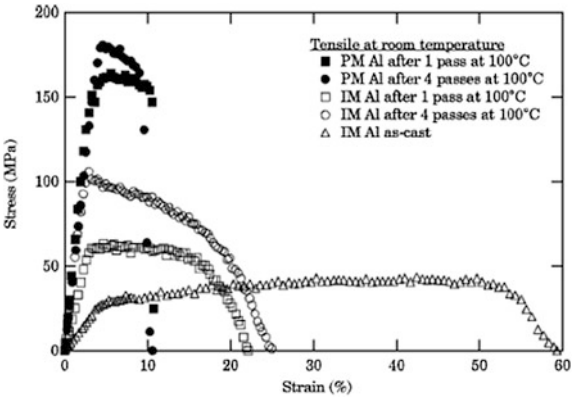

Fig. 1.13 Tensile curves for pure bulk (IM) and powdered (PM) Al samples processed/consolidated by ECAP [147]

Fully dense bulk material are produced thanks to the material flow accompanying the deformation, which is believed to be able to close the pores between the particles [157]. Since ECAP is not a high-temperature slow-diffusion consolidation process, it can be performed at much lower temperatures and shorter processing times than conventional sintering process. ECAP consolidated samples showed remarkably high yield strength and hardness compared to their ingot counterparts due to their fine and equiaxed microstructure [6, 147, 158], as shown in Fig. 1.13 [147].

The application of BP is very useful during ECAP consolidation of powdered materials at low temperatures, especially when cans are not used. Shearing of individual particles and fracturing of the surface oxide layer are the prerequisite for SPD powder consolidation [6]. With the application of a BP, the particles are pushed against each other, generating more friction when passing the shear zone and causing the particles to shear deform more efficiently instead of just sliding on each other.

1.2.3 Hot Extrusion

Extrusion is a process used to produce parts with fixed cross-section (bars, wires, billets, profiles, tubes). There are two main types of extrusion processes:

- direct extrusion: a plunger pushes a workpiece forward through a die, causing a reduction in cross-sectional area of the workpiece.
- indirect or inverted extrusion: the metal is contained in a blind cylinder, the plunger which houses the die compresses the metal against the container, forcing it to flow backward to the die in the hollow plunger.

The extrusion process can be done at low or, more frequently, at high temperatures to improve material plasticity. The great advantage of the extrusion process lies in the relative ease and efficiency with which complex sections can be produced in one operation. A schematic representation of the direct extrusion process is depicted in Fig. 1.14. The reduction of cross section (reduction ratio, R) of the extruded part can be calculated as follow:

$$R = \frac{A_0}{A_f} \tag{1.16}$$

where A_0 and A_f are the cross areas of the billet before and after extrusion, respectively [159].

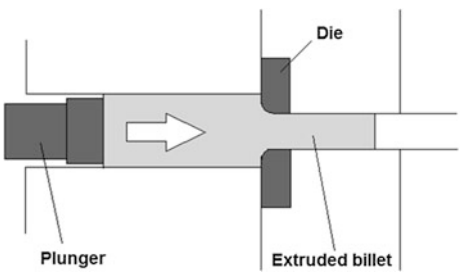

Fig. 1.14 Schematic of the direct extrusion process

1.2.3.1 Extrusion Process Variables

The force needed for extrusion is affected by a variety of circumstances. Mainly, it is affected by the nature of the material, by the temperature and by the speed at which the extrusion is performed. Moreover, the amount of deformation involved must be considered, i.e. the reduction ratio. Additional factors are the shape of the section and the design of the die used. For pure aluminum and the soft alloys, for example, reduction ratios of up to 100:1 are not uncommon, while for the hard alloys the ratio is usually between 8:1 and 40:1. The speed of extrusion depends upon the available pressure and thus on the alloy temperature and reduction ratio [159].

1.2.3.2 Consolidation of Particles by Extrusion

Pioneering experiments on the extrusion of metal powders were carried out in the late 1950s [160]. In principle, both direct and indirect extrusion methods may be used to extrude metal powders, but direct extrusion is much more widely used. For this reason, this section will only focus on direct extrusion. During extrusion, metal powders undergo plastic deformation, usually at high temperatures, to produce a full dense form. The three main routes to extrude powders are depicted in Fig. 1.15. In the first method, a hot container supplies heat to the charge and extrusion is performed without atmosphere protection. The second method relies on the use of a precompacted billet, referred as a "green compact", as the extrusion workpiece.

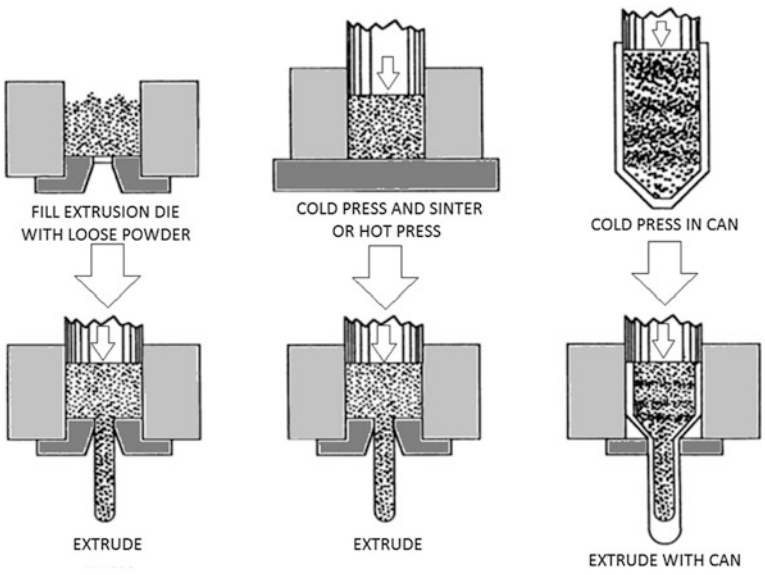

Fig. 1.15 Three main routes to extrude metal powders [161]

Cold or hot pressing are suitable process for producing green compacts. However, sintering is not a required processing step and many materials are extruded without this additional processing. The third approach consists in partially densifying the metal powder in a can. This may then be evacuated and sealed, or it may be left open to the atmosphere [161].

Canning can be employed for the following advantages [162]:

- isolation of the powdered material from the atmosphere and lubricants: it is a clean extrusion technique;
- isolation of toxic materials for safe handling;
- encapsulation of spherical and other difficult-to-compact powders to produce a billet form;
- reduction of friction and facilitation of metal flow at the die interface by proper selection of the can material;
- isolation of the powdered material from the extrusion channel, which is the region of highest shear. It is an important consideration for materials with limited ductility.
- capability of positioning powders and solid components within the can to produce unique and complex shapes.

When purity must be maintained, canning of the powder, including gas evacuation and sealing, is an essential step [97, 163]. Procedures may include glove box container preparation and assembly, total isolation of powder from ambient air, evacuation at slightly elevated temperatures to drive off adsorbed gases from particle surfaces, and leak checking of sealed containers. Sometime, a requirement is that the extruded product must be free from both particle native oxide layers and nonmetallic inclusions that can degrade some mechanical properties, like fracture toughness and fatigue resistance [161, 162].

1.3 Possible Applications of MMnCs

So far, to the author' best knowledge, metal matrix composites reinforced by nanoparticles or nanotubes are not being employed yet in relevant commercial applications due to their very recent development. However, MMnCs show higher mechanical properties than micro-particles reinforced composites, without any evidence of a strong drop in thermal and electrical conductivity [5, 6]. For this reason, they are considered as possible candidates for substituting conventional MMCs or related monolithic alloys in structural and electrical applications at room and high temperatures. For example, CNT composites could replace, thanks to their higher strength and stiffness, carbon fibers composite in many applications, especially in high-temperature environments. Another good opportunity for the substitution of traditional MMCs with nano-sized counterparts is related to the good fracture toughness and ductility, which was the main Achille's heel in micro-reinforced MMCs. Toughness can be substantially preserved in nano-reinforced

composites owing to the reduced particle volume fraction required to achieve strengthening, thus widening the opportunity for structural applications, even in highly demanding and safety parts.

For instance, the enhanced wear resistance [9] and the good thermal conductivity combined to the high specific strength make MMnCs attractive materials for aircraft brakes. Moreover, the specific strength and elastic modulus could be exploited in sport industry, for instance for rackets or bicycle frames and other components. A further field of potential application is in electronic devices, for example for heat sinks and solders (thanks to their thermal properties) or as antennas (thanks to their electrical properties and stiffness). Aerospace and automotive industries may exploit all the above properties for different kind of applications such as structural radiators, gears, aircraft fins, cylinder liners, pistons, disk brakes and calipers.

The improved damping capacity of MMnCs could also be exploited to reduce vibrations and noise of structures. In Mg-Al_2O_3 samples extruded at 350 °C after powder milling, a significant damping ability was highlighted and attributed to interface character of MMnCs [7].

References

1. S.C. Tjong, Novel nanoparticle-reinforced metal matrix composites with enhanced mechanical properties. Adv. Eng. Mater. **9**, 639–652 (2007)
2. R. Casati, M. Vedani, Metal matrix composites reinforced by nano-particles—a review. Metals **4**(1), 65–83 (2014)
3. C.F. Deng, D.Z. Wang, X.X. Zhang, Y.X. Ma, Damping characteristics of carbon nanotube reinforced aluminum composite. Mater. Lett. **61**, 3229–3231 (2007)
4. V.C. Nardone, K.M. Prewo, On the strength of discontinuous silicon carbide reinforced aluminum composites. Scr. Metall. **20**, 43–48 (1986)
5. C. Xu, K. Xia, T.G. Langdon, The role of back pressure in the processing of pure aluminum by equal-channel angular pressing. Acta Mater. **55**, 2351–2360 (2007)
6. X. Wu, K. Xia, Back pressure equal channel angular consolidation—Application in producing aluminum matrix composites with fine flyash particles. J. Mater. Process. Technol. **192–193**, 355–359 (2007)
7. S. Goussous, W. Xu, X. Wu, K. Xia, Al-C nanocomposites consolidated by back pressure equal channel angular pressing. Comput. Sci. Technol. **69**, 1997–2001 (2009)
8. W. Xu, X. Wu, T. Honma, S.P. Ringer, K. Xia, Nanostructured Al–Al_2O_3 composite formed in situ during consolidation of ultrafine Al particles by back pressure equal channel angular pressing. Acta Mater. **57**, 4321–4330 (2009)
9. Y. Li, Y.H. Zhao, V. Ortalan, W. Liu, Z.H. Zhang, R.G. Vogt, N.D. Browning, E.J. Lavernia, J.M. Schoenung, Investigation of aluminum-based nanocomposites with ultra-high strength. Mater. Sci. Eng. A **527**, 305–316 (2009)
10. S. Goussous, W. Xu, K. Xia, Developing aluminum nanocomposites via severe plastic deformation. J. Phys: Conf. Ser. **240**, 012106 (2010)
11. M. Kubota, X. Wu, W. Xu, K. Xia, Mechanical properties of bulk aluminium consolidated from mechanically milled particles by back pressure equal channel angular pressing. Mater. Sci. Eng. A **527**, 6533–6536 (2010)
12. F. He, Q. Han, M.J. Jackson, Nanoparticulate reinforced metal matrix nanocomposites—a review. Int. J. Nanopart. **1**, 301–309 (2008)

13. X. Li, Y. Yang, X. Cheng, Ultrasonic-assisted fabrication of metal matrix nanocomposites. J. Mater. Sci. **39**, 3211–3212 (2004)
14. S.X. Mao, N.A. McMinn, N.Q. Wu, Processing and mechanical behavior of TiAl/NiAl intermetallic composites produced by cryogenic emchnical alloying. Mater. Sci. Eng. A **363**, 275–289 (2003)
15. H. Mahboob, S. A. Sajjadi, S.M. Zebarjad, Syntesis of Al-Al_2O_3 nanocomposite by mechanical alloying and evaluation of the effect of ball milling time on the microstructure and mechanical properties, in *Proceedings of International Conference on MEMS and Nanotechnology* (*ICMN '08*). Kuala Lumpur, Malaysia, pp. 240–245, 13–15 May 2008
16. M. Gupta, M.O. Lai, C.Y. Soo, Effect of type of processing on the microstructural features and mechanical properties of Al-Cu/SiC metal matrix composites. Mater. Sci. Eng. A **210**, 114–122 (1996)
17. L. Lu, M.O. Lai, Y. Su, H.L. Teo, C.F. Feng, In situ TiB_2 reinforced Al alloy composites. Scripta Mater. **45**, 1017–1023 (2001)
18. M. Gupta, M.O. Lai, M.S. Boon, N.S. Herng, Regarding the SiC particulates size associated microstructural characteristics on the aging behavior of Al-4.5 Cu metallic matrix. Mater. Res. Bull. **33**, 199–209 (1998)
19. A.M.K. Esawi, K. Morsi, A. Sayed, A. Abdel Gawad, P. Borah, Fabrication and properties of dispersed carbon nanotube-aluminum composites. Mater. Sci. Eng. A. **508**, 167–173 (2009)
20. C.F. Deng, D.Z. Wang, X.X. Zhang, A.B. Li, Processing and properties of carbon nanotubes reinforced aluminum composites. Mater. Sci. Eng. A. **444**, 138–145 (2007)
21. R. Derakhshandeh Haghighi, S.A. Jenabali Jahromi, A. Moresedgh, M. Tabandeh Khorshid, A comparison between ECAP and conventional extrusion for consolidation of aluminum metal matrix composite. J. Mater. Eng. Perform. **21**, 1885–1892 (2012)
22. C. Carreño-Gallardo, I. Estrada-Guel, M. Romero-Romo, R. Cruz-García, C. López-Meléndez, R. Martínez-Sánchez, Characterization of Al_2O_3 NP–Al2024 and AgCNP–Al2024 composites prepared by mechanical processing in a high energy ball mill. J. Alloy. Compd. **536**, S26–S30 (2012)
23. M. Tavoosi, F. Karimzadeh, M.H. Enayati, Fabrication of Al-Zn/α-Al_2O_3 nanocomposite by mechanical alloying. Mater. Lett. **62**, 282–285 (2008)
24. L. Kollo, M. Leparoux, C.R. Bradbury, C. Jäggi, E. Carreño-Morelli, M. Rodríguez-Arbaizar, Investigation of planetary milling for nano-silicon carbide reinforced aluminium metal matrix composites. J. Alloy. Compd. **489**, 394–400 (2010)
25. L. Lu, M.O. Lai, J.L. Yeo, In situ synthesis of TiC composite for structural application. Compos. Struct. **47**, 613–618 (1999)
26. R. Derakhshandeh, H.A. Jenabali Jahromi, An investigation on the capability of equal channel angular pressing for consolidation of aluminum and aluminum composite powder. Mater. Des. **32**, 3377–3388 (2011)
27. M. De Cicco, L. Turng, X. Li, J.H. Perepezko, Nucleation catalysis in Aluminum alloy A356 using nanoscale inoculants. Metall. Mater. Trans. A **42**, 2323–2330 (2011)
28. M. De Cicco, L. Turng, X. Li, J.H. Perepezko, Production of semi-solid slurry through heterogeneous nucleation in metal matrix nanocomposites (MMNC) using nano-scaled ultrasonically dispersed inoculants. Solid State Phenom **141–143**, 487–492 (2008)
29. J. Li, W. Xu, X. Wu, H. Ding, K. Xia, Effects of grain size on compressive behaviour in ultrafine grained pure Mg processed by equal-channel angular pressing at room temperature. Mater. Sci. Eng. A **528**, 5993–5998 (2011)
30. A. Erman, J. Groza, X. Li, H. Choi, G. Cao, Nanoparticle effects in cast Mg-1 wt% SiC nano-composites. Mater. Sci. Eng. A **558**, 39–43 (2012)
31. Z. Wang, X. Wang, Y. Zhao, W. Du, SiC nanoparticles reinforced magnesium matrix composites fabricated by ultrasonic method. Trans. Nonferrous Met. Soc. China **20**, s1029–s1032 (2010)
32. H. Frenkel, B.L. Mordike, Magnesium strengthened by SiC nanoparticles. Mater. Sci. Eng. A **298**, 193–199 (2001)

33. K.B. Nie, X.J. Wang, L. Xu, K. Wu, X.S. Hu, M.Y. Zheng, Influence of extrusion temperature and process parameter on microstructures and tensile properties of a particulate reinforced magnesium matrix nanocomposites. Mater. Des. **36**, 199–205 (2012)
34. G. Cao, H. Choi, J. Oportus, H. Konishi, X. Li, Study on tensile properties and microstructure of cast AZ91D/AlN nanocomposites. Mater. Sci. Eng. A **494**, 127–131 (2008)
35. Q. Li, C.A. Rottmair, R.F. Singer, CNT reinforced light metal composites produced by melt stirring and by high pressure die casting. Compos. Sci. Technol. **70**, 2242–2247 (2010)
36. M.O. Lai, L. Lu, W. Laing, Formation of magnesium nanocomposite via mechanical milling. Compos. Struct. **66**, 301–304 (2004)
37. Kwangmin Choi, Jiyeon Seo, Donghyun Bae, Hyunjoo Choi, Mechanical properties of aluminum-based nanocomposite reinforced with fullerenes. Trans. Nonferrous Met. Soc. China **24**, s47–s52 (2014)
38. P. Luo, D.T. McDonald, W. Xu, S. Palanisamy, M.S. Dargusch, K. Xia, A modified Hall-Petch relationship in ultrafine-grained titanium recycled from chips by equal channel angular pressing. Scripta Mater. **66**, 785–788 (2012)
39. P. Luo, D.T. McDonald, S.M. Zhu, S. Palanisamy, M.S. Dargusch, K. Xia, Analysis of microstructure and strengthening in pure titanium recycled from machining chips by equal-channel angular pressing using electron backscatter diffraction. Mater. Sci. Eng. A **538**, 252–258 (2012)
40. V.V. Stolyarov, Y.T. Zhu, I.V. Alexandrov, T.C. Lowe, R.Z. Valiev, Influence of ECAP routes on the microstructure and properties of pure Ti. Mater. Sci. Eng. A **299**, 59–67 (2001)
41. S.M. Uddin, T. Mahmud, C. Wolf, C. Glanz, I. Kolaric, C. Volkmer, H. Höller, U. Wienecke, S. Roth, H. Fecht, Effect of size and shape of metal particles to improve hardness and electrical properties of carbon nanotube reinforced copper and copper alloy composites. Compos. Sci. Technol. **70**, 2253–2257 (2010)
42. D. Bozic, J. Stasic, B. Dimcic, M. Vilotijevic, V. Rajkovic, Multiple strengthening mechanisms in nanoparticle-reinforced copper matrix composites. J. Mater. Sci. **34**, 217–226 (2011)
43. J. Naser, W. Riehemann, H. Frenkel, Dispersion hardening of metals by nanoscaled ceramic powders. Mater. Sci. Eng. A **234–236**, 467–469 (1997)
44. P. Quang, Y.G. Jeong, S.C. Yoon, S.H. Hong, H.S. Kim, Consolidation of 1 vol.% carbon nanotube reinforced metal matrix nanocomposites via equal channel angular pressing. J. Mater. Process. Technol. **187–188**, 318–320 (2007)
45. H. Ahamed, V. Senthilkumar, Consolidation behavior of mechanically alloyed aluminum based nanocomposites reinforced with nanoscaled Y_2O_3/Al_2O_3. Mater. Charact. **62**, 1235–1249 (2011)
46. S.R. Bakshi, D. Lahiri, A. Agarwal, Carbon nanotube reinforced metal composites-a review. Int. Mater. Rev. **55**, 42–64 (2010)
47. S.S. Nayak, S.K. Pabi, D.H. Kim, B.S. Murty, Microstructure-hardness relationship of Al–$(L1_2)Al_3Ti$ nanocomposites prepared by rapid solidification processing. Intermetallics **18**, 487–492 (2010)
48. E.O. Hall, The deformation and aging of mild steel. Proc. Phys. Soc. London, Sec. B **64**, 747–753 (1951)
49. N.J. Petch, The cleavage strength of polycrystals. J. Iron Steel Res. **174**, 25–28 (1953)
50. D. Hull, D.J. Bacon, *Introduction to Dislocations*, 4th edn. (Butterworth-Heinemann, London, 2001)
51. D. Hull, T.W. Clyne, An Introduction to Composite Materials. Cambridge Solid State Science Series. 2th edn. (1996)
52. A. Sanaty-Zadeh, Comparison between current models for the strength of particulate-reinforced metal matrix nanocomposites with emphasis on consideration of Hall-Petch effect. Mater. Sci. Eng. A **531**, 112–118 (2012)
53. Z. Zhang, D.L. Chen, Contribution of Orowan strengthening effect in particulate-reinforced metal matrix nanocomposites. Mater. Sci. Eng. A **483–484**, 148–152 (2008)

54. Z. Zhang, D.L. Chen, Consideration of Orowan strengthening effect in particulate-reinforced metal matrix nanocomposites: a model for predicting their yield strength. Scripta Mater. **54**, 1321–1326 (2006)
55. A.H. Chokski, A. Rosen, J. Karch, H. Gleiter, On the validity of the Hall–Petch relationship in nanocrystalline materials'. Scr. Metall. **23**, 1679–1683 (1989)
56. G.W. Nieman, J.R. Weertman, R.W. Siegel, Microhardness of nanocrystallinepalladium and copper produced by inert-gas condensation. Scr. Metall. **23**, 2013–2018 (1989)
57. K. Lu, W.D. Wei, J.T. Wang, Microhardness and fracture properties of nanocrystalline Ni–P alloy. Scr. Metall. Mater. **24**, 2319–2323 (1990)
58. G.W. Nieman, J.R. Weertman, R.W. Siegel, Mechanical behavior of nanocrystalline Cu and Pd. J. Mater. Res. **6**, 1012–1027 (1991)
59. G.E. Fougere, J.R. Weertman, R.W. Siegel, S. Kim, Grain-size dependent hardening and softening of nanocrystalline Cu and Pd. Scr. Metall. Mater. **26**, 1879–1883 (1992)
60. A.M. El-Sherik, U. Erb, G. Palumbo, K.T. Aust, Deviations from Hall-Petch behavior in as-prepared nanocrystalline nickel. Scr. Metall. Mater. **27**, 1185–1188 (1992)
61. V.Y. Gertsman, M. Hoffmann, H. Gleiter, R. Dirringer, The study of grain size dependence of yield of copper. Acta Metall. Mater. **42**, 3539–3544 (1994)
62. P.G. Sanders, J.A. Eastman, J.R. Weertman, Elastic and tensile behavior of nanocrystalline copper and palladium. Acta Mater. **45**, 4019–4025 (1997)
63. N. Wang, Z. Wang, K.T. Aust, U. Erb, Room temperature creep behavior of nanocrystalline nickel produced by an electrodeposition technique. Mater. Sci. Eng. A. **237**, 150–158 (1997)
64. C.A. Schuh, T.G. Nieh, T. Yamasaki, Hall-Petch breakdown manifested in abrasive wear resistance of nanocrystalline nickel. Scripta Mater. **46**, 735–740 (2002)
65. A. Giga, Y. Kimoto, Y. Takigawa, K. Higashi, Demonstration of an inverse Hall-Petch relationship in electrodeposited nanocrystalline Ni–W alloys through tensile testing. Scripta Mater. **55**, 143–146 (2006)
66. C.E. Carlton, P.J. Ferreira, What is Behind the Inverse Hall-Petch effect in nanocrystalline materials? Acta Mater. **55**, 3749–3756 (2007)
67. Z.Y. Ma, Y.L. Li, Y. Liang, F. Zheng, J. Bi, S.C. Tjong, Nanometric Si_3N_4 particulate-reinforced aluminum composite. Mater. Sci. Eng. A **219**, 229–231 (1996)
68. D.J. Lloyd, Particle-reinforced aluminum and magnesium matrix composites. Int. Mater. Rev. **39**, 1–23 (1994)
69. N.A. Fleck, M.F. Ashby, J.W. Hutchinson, The role of geometrically necessary dislocations ingiving material strengthening. Scripta Mater. **48**, 179–183 (2003)
70. R.J. Arsenault, N. Shi, Dislocation generation due to differences between the coefficients of thermal-expansion. Mater. Sci. Eng. A **81**, 175–187 (1986)
71. R.E. Smallman, A.H.W. Ngan, Physical Metallurgy and Advanced Materials, 7th edn (Butterworth-Heinemann, London, 2007)
72. M.A. Azouni, P. Casses, Thermophysical properties effects on segregation during solidification. Adv. Colloid Interface Sci. **75**, 83–106 (1998)
73. J. Lan, Y. Yang, X. Li, Microstructure and microhardness of SiC nanoparticles reinforced magnesium composites. Mater. Sci. Eng. A **386**, 284–290 (2004)
74. G. Cao, J. Kobliska, H. Konishi, X. Li, Tensile properties and microstructure of SiC nanoparticle-reinforced Mg-4Zn alloy fabricated by ultrasonic cavitation-based solidification processing. Metall. Mater. Trans. A **39**, 880–886 (2008)
75. Chapter Insight into Designing Biocompatible Magnesium Alloys and Composites Part of the series SpringerBriefs in Materials, pp. 17–34 Date: 15 January 2015 Synthesis of Magnesium-Based Biomaterials
76. N. Srikanth, K.F. Ho, M. Gupta, Effect of length scale of alumina particles of different sizes on the damping characteristics of an Al–Mg alloy. Mater. Sci. Eng. A **423**, 189–191 (2006)
77. D. Gu, Y.C. Hagedoorn, W. Meiners, K. Wissenbach, R. Poprawe, Nanocrystalline TiC reinforced Ti matrix bulk-form nanocomposites by selective laser melting (SLM): densification, growth mechanism and wear behavior. Compos. Sci. Technol. **71**, 1612–1620 (2011)

78. J.P. Tu, N.Y. Wang, Y.Z. Yang, W.X. Qi, F. Liu, X.B. Zhang, H.M. Lu, M.S. Liu, Preparation and properties of TiB_2 nanoparticles reinforced copper matrix composites by in situ processing. Mater. Lett. **52**, 448–452 (2002)
79. N.L. Yue, L. Lu, M.O. Lai, Application of thermodynamic calculation in the in-situ process of Al/TiB_2. Compos. Struct. **47**, 691–694 (1999)
80. Y.Q. Liu, H.T. Cong, W. Wang, C.H. Sun, H.M. Cheng, AlN nanoparticle-reinforced nanocrystalline Al matrix composites: fabrication and mechanical properties. Mater. Sci. Eng. A **505**, 151–156 (2009)
81. Z. Bian, M.X. Pan, Y. Zhang, W.H. Wang, Carbon-nanotube-reinforced $Zr_{52.5}Cu_{17.9}Ni_{14.6}Al_{10}Ti_5$ bulk metallic glass composites. Appl. Phys. Lett. **81**, 4739–4741 (2002)
82. Z. Bian, R.J. Wang, W.H. Wang, T. Zhang, A. Inoue, Carbon-nanotube-reinforced Zr-based bulk metallic glass composites and their properties. Adv. Funct. Mater. **14**, 55–63 (2004)
83. C.S. Goh, J. Wei, L.C. Lee, M. Gupta, Ductility improvement and fatigue studies in Mg-CNT nanocomposites. Compos. Sci. Technol. **68**, 1432–1439 (2008)
84. E. El-Kady, T. Mahmoud, A. Ali, On the electrical and thermal conductivities of Cast A356/Al_2O_3 metal matrix nanocomposites. Mater. Sci. Appl. **22**, 1180–1187 (2011)
85. M. De Cicco, X. Li, L.S. Turng, Semi-solid casting (SSC) of zinc alloy nanocomposites. J. Mater. Process. Technol. **209**, 5881–5885 (2009)
86. L. Lu, M.O. Lai, Formation of new materials in the solid state by mechanical alloying. Mater. Des. **16**, 33–39 (1995)
87. F. Zhang, W.A. Kacmarek, L. Lu, M.O. Lai, Formation of Al TiN metal matrix composite via mechanochemical route. Scripta Mater. **43**, 1097–1102 (2000)
88. M. Mozaffari, M. Gheisari, M. Niyaifar, J. Amighian, Magnetic properties of mechanochemically prepared iron-wustite (Fe-FeyO) nanocomposites. J. Magn. Magn. Mater. **321**, 2981–2984 (2009)
89. Z. Razavi Hesabi, A. Simchi, S.M. Seyed Reihani, Structural evolution during mechanical milling of nanometric and micrometric Al_2O_3 reinforced Al matrix composites. Mater. Sci. Eng. A **428**, 159–168 (2006)
90. L. Lu, M.O. Lai, Y.H. Toh, L. Froyen, Structure and properties of Mg-Al-Ti-B alloys synthesized via mechanical alloying. Mater. Sci. Eng. A **334**, 163–172 (2002)
91. E. Mostaed, H. Saghafian, A. Mostaed, A. Shokuhfar, H.R. Rezaie, Investigation on preparation af Al-4.5 %Cu/SiCp nanocomposites powder via mechanical milling. Powder Technol. **221**, 278–283 (2012)
92. L. Lu, M.O. Lai, W. Liang, Magnesium nanocomposites via mechanochemical milling. Compos. Sci. Technol. **64**, 2009–2014 (2004)
93. M.A. Thein, L. Lu, M.O. Lai, Effect of milling and reinforcement on mechanical properties of nanostructured magnesium composite. J. Mater. Process. Technol. **209**, 4439–4443 (2009)
94. R. Casati, Q. Ge, M. Vedani, D. Dellasega, P. Bassani, A. Tuissi, Preparazione di nano-compositi a matrice metallica Al/Al_2O_3 mediante ECAP e estrusione a caldo. La Metallurgia Italiana **105**, 25–30 (2013)
95. F. Shehata, A. Fathy, M. Abdelhameed, S.F. Mustafa, Preparation and properties of Al_2O_3 nanoparticle reinforced copper matrix composites by in situ processing. Mater. Des. **30**, 2756–2762 (2009)
96. Z. Trojanova, P. Lukac, H. Ferkel, W. Riehemann, Internal friction in microcrystalline and nanocrystalline Mg. Mater. Sci. Eng. A **370**, 154–157 (2004)
97. R. Casati, F. Bonollo, D. Dellasega, A. Fabrizi, G. Timelli, A. Tuissi, M. Vedani, Ex situ Al-Al_2O_3 ultrafine grained nanocomposites produced via powder metallurgy. J. Alloy. Compd. **615**, S386–S388 (2014)
98. R. Casati, M. Amadio, C.A. Biffi, D. Dellasega, A. Tuissi, M. Vedani, Al/Al_2O_3 nano-composite produced by ECAP. Mater. Sci. Forum. **762**, 457–464 (2013)
99. X. Xia, Consolidation of particles by severe plastic deformation: mechanism and applications in processing bulk ultrafine and nanostructured alloys and composites. Adv. Eng. Mater. **12**, 724–729 (2010)

100. R. Derakhshande, H.S.A. Jenabali Jahromi, B. Esfandiar. Simulation aluminum powder in tube compaction using equal channel angular pressing. J. Mater. Eng. Perform. **21**, 143–152 (2012)
101. C. Suryanarayana, Mechanical alloying and milling. Prog. Mater Sci. **46**, 1–184 (2001)
102. S.C. Tjong, H. Chen, Nanocrystalline materials and coatings. Mater. Sci. Eng. R. **45**, 1–88 (2004)
103. J. Benjamin, Mechanical alloying. Sci. Am. **234**, 40–49 (1976)
104. P.Y. Lee, J.L. Yang, H.M. Lin, Amorphization behaviour in mechanically alloyed Ni—Ta powders. J. Mater. Sci. **33**, 235–239 (1998)
105. J.S. Benjamin, T.E. Volin, Mechanism of mechanical alloying. Metall. Trans. **5**, 1929–1934 (1974)
106. P.S. Gilman, J.S. Benjamin, Mechanical alloying. Annu. Rev. Mater. Sci. **13**, 279–300 (1983)
107. J.S. Benjamin, Mechanical alloying—A perspective. Met. Powder Rep. **45**, 122–127 (1990)
108. C. Suryanarayana, E. Ivanov, R. Noun, M.A. Contreras, J.J. Moore, Phase selection in a mechanically alloyed Cu-In-Ga-Se powder mixture. J. Mater. Res. **14**, 377–383 (1999)
109. B.L. Chu, C.C. Chen, T.P. Perng, Amorphization of Ti_{1-x} Mn_x. Metall. Trans. A. Phys. Metall. Mater. Sci. **23**, 2105–2110 (1992)
110. K. Tokumitsu, Synthesis of metastable Fe_3C, Co_3C and Ni_3C by mechanical alloying method. Mater. Sci. Forum **235–238**, 127–132 (1997)
111. B.K. Yen, T. Aizawa, J. Kihara, Synthesis and formation mechanisms of molybdenum silicides by mechanical alloying. Mater. Sci. Eng. A **220**, 8–14 (1996)
112. B.K. Yen, T. Aizawa, J. Kihara, Mechanical alloying behavior in molibdenum-silicon system. Mater. Sci. Forum. **235–238,** 157–162 (1997)
113. A. Tonejc, D. Duzevic, A.M. Tonejc, Effects of ball milling on pure antimony, on Ga—Sb alloy and on Ga + Sb powder mixture; oxidation, glass formation and crystallization. Sci. Eng. A **134**, 1372–1375 (1991)
114. T. Ohtani, K. Maruyama, K. Ohshima, Synthesis of copper, silver, and samarium chalcogenides by mechanical alloying. Mater. Res. Bull. **32**, 343–350 (1997)
115. W. Guo, A. Iasonna, M. Magini, S. Martelli, F. Padella, Synthesis of amorphous and metastable $Ti_{40}Al_{60}$ alloys by mechanical alloying of elemental powders. J. Mater. Sci. **29**, 2436–2444 (1994)
116. F. Padella, E. Paradiso, N. Burgio, M. Magini, S. Martelli, W. Guo, A. Iasonna, Mechanical alloying of the Pd-Si system in controlled conditions of energy transfer. J. Less Common Metals **175**, 79–90 (1991)
117. K.B. Gerasimov, A.A. Gusev, E.Y. Ivanov, V.V. Boldyrev, Tribochemical equilibrium in mechanical alloying of metals. J. Mater. Sci. **26**, 2495–2500 (1991)
118. L. Liu, S. Casadio, M. Magini, C.A. Nannetti, Y. Qin, K. Zheng, Solid state reactions of $V_{75}Si_{25}$ driven by mechanical alloying. Mater. Sci. Forum **235–238**, 163–168 (1997)
119. L. Takacs, M. Pardavi-Horvath, Nanocomposite formation in the Fe_3O_4-Zn system by reaction milling. J. Appl. Phys. **75**, 5864–5866 (1994)
120. W.E. Frazier, M.J. Koczak, Mechanical and thermal stability of powder metallurgy aluminum-titanium alloys. Scr. Metall. **21**, 129–134 (1987)
121. G. Chen, K. Wang, J. Wang, H. Jiang, M. Quan. In: deBarbadillo, J.J. et al. (Eds). Mechanical alloying for structural applications. ASM International, Materials Park, OH, 1993) pp. 183–187
122. P.K. Ivison, N. Cowlam, I. Soletta, G. Cocco, S. Enzo, L. Battezzati, The influence of hydrogen contamination on the amorphization reaction of CuTi alloys. Mater. Sci. Eng. A **134**, 859–862 (1991)
123. P.K. Ivison, I. Soletta, N. Cowlam, G. Cocco, S. Enzo, L. Battezzati, Evidence of chemical short-range order in amorphous CuTi alloys produced by mechanical alloying. J. Phys.: Condens. Matter. **4**, 1635–1645 (1992)

124. L.B. Hong, C. Bansal, B. Fultz, Steady state grain size and thermal stability of nanophase Ni_3Fe and Fe_3X (X=Si, Zn, Sn) synthesized by ball milling at elevated temperatures. Nanostruct. Mater. **4**, 949–956 (1994)
125. C.C. Koch, D. Pathak, K. Yamada. In: deBarbadillo JJ, et al. (Eds) Mechanical alloying for structural applications. (ASM International, Materials Park, OH, 1993), pp. 205–212
126. H. Kimura, M. Kimura, in *Solid State Powder Processing*, ed. by A.H. Clauer, J. J. deBarbadillo (TMS, Warrendale, PA, 1990), pp. 365–377
127. C.H. Lee, M. Mori, T. Fukunaga, U. Mizutani, Effect of ambient temperature on the MA and MG processes in Ni–Zr alloy system. Jpn. J. Appl. Phys. **29**, 540–544 (1990)
128. V.M. Segal, Methods of stress-strain analysis in metalforming. (Physical Technical Institute Academy of Sciences of Buelorussia, Minsk, Russia, 1974)
129. R.Z. Valiev, N.A. Krasilnikov, N.K. Tsenev, Plastic-deformation of alloys with submicron-grained structure. Mater. Sci. Eng. A **137**, 35–40 (1991)
130. R.Z. Valiev, A.V. Korznikov, R.R. Mulyukov, Structure and properties of ultrafine-grained materials produced by severe plastic-deformation. Mater. Sci. Eng. A **168**, 141–148 (1993)
131. V.M. Segal, Engineering and commercialization of equal channel angular extrusion (ECAE). Mater. Sci. Eng. A **386**, 269–276 (2004)
132. R.Z. Valiev, R.K. Islamgaliev, I.V. Alexandrov, Bulk nanostructured materials from severe plastic deformation. Prog. Mater Sci. **45**, 103–189 (2000)
133. Y. Iwahashi, Z. Horita, M. Nemoto, T.G. Langdon, An investigation of microstructural evolution during equal-channel angular pressing. Acta Mater. **45**, 4733–4741 (1997)
134. Y. Iwahashi, J. Wang, Z. Horita, M. Nemoto, T.G. Langdon, Principle of equal-channel angular pressing for the processing of ultra-fine grained materials. Scripta Mater. **35**, 143–146 (1996)
135. V.M. Segal, Equal channel angular extrusion: from macromechanics to structure formation. Mater. Sci. Eng. A **271**, 322–333 (1999)
136. R.Z. Valiev, T.G. Langdon, Principles of equal-channel angular pressing as a processing tool for grain refinement. Prog. Mater Sci. **51**, 881–981 (2006)
137. Y. Iwahashi, Z. Horita, M. Nemoto, T.G. Langdon, The process of grain refinement in equal-channel angular pressing. Acta Mater. **46**, 3317–3331 (1998)
138. T.G. Langdon, The characteristics of grain refinement in materials processed by severe plastic deformation. Rev. Adv. Mater. Sci. **13**, 6–14 (2006)
139. R.Z. Valiev, T.G. Langdon, Developments in the use of ECAP processing for grain refinement. Rev. Adv. Mater. Sci. **13**, 15–26 (2006)
140. R.Z. Valiev, R.K. Islamgaliev, N.F. Kuzmina, T.G. Langdon, Strengthening and grain refinement in an Al-6061 metal matrix composite through intense plastic straining. Scripta Mater. **40**, 117–122 (1998)
141. I. Gutierrez-Urrutia, M.A. Munoz-Morris, D.G. Morris, The effect of coarse second-phase particles and fine precipitates on microstructure refinement and mechanical properties of severely deformed Al alloy. Mater. Sci. Eng. A **394**, 399–410 (2005)
142. K. Nakashimaa, Z. Horitaa, M. Nemoto, T.G. Langdon, Development of a multi-pass facility for equal-channel angular pressing to high total strains. Mater. Sci. Eng. A **281**, 82–87 (2000)
143. A. Yamashita, D. Yamaguchia, Z. Horitaa, T.G. Langdonb, Influence of pressing temperature on microstructural development in equal-channel angular pressing. Mater. Sci. Eng. A **287**, 100–106 (2000)
144. D.H. Shin, J.J. Pak, Y.K. Kim, K.T. Park, Y.S. Kim, Effect of pressing temperature on microstructure and tensile behavior of low carbon steels processed by equal channel angular pressing. Mater. Sci. Eng. A **325**, 31–37 (2002)
145. Y.C. Chen, Y.Y. Huang, C.P. Chang, P.W. Kao, The effect of extrusion temperature on the development of deformation microstructures in 5052 aluminium alloy processed by equal channel angular extrusion. Acta Mater. **51**, 2005–2015 (2003)
146. W.H. Huang, C.Y. Yu, P.W. Kao, C.P. Chang, The effect of strain path and temperature on the microstructure developed in copper processed by ECAE. Mater. Sci. Eng. A **366**, 221–228 (2004)

147. K. Xia, X. Wu, T. Honma, S.P. Ringer, Ultrafine pure aluminium through back pressure equal channel angular consolidation (BP-ECAC) of particles. J. Mater. Sci. **42**, 1551–1560 (2007)
148. W. Xu, T. Honma, X. Wu, S.P. Ringer, High strength ultrafine/nanostructured aluminum produced by back pressure equal channel angular processing. Appl. Phys. Lett. **91**, 031901 (2007)
149. A. Bohner, F. Kriebel, R. Lapovok, H.W. Höppel, M. Göken, Influence of backpressure during ECAP on the monotonic and cyclic deformation behavior of Aa_{5754} and $Cu_{99.5}$. Adv. Eng. Mater. **13**, 269–274 (2011)
150. R.Y. Lapovok, The role of back-pressure in equal channel angular extrusion. J. Mater. Sci. **40**, 341–346 (2005)
151. P.W.J. McKenzie, R. Lapovok, Y. Estrin, The influence of back pressure on ECAP processed. AA 6016: modeling and experiment. Acta Mater. **55**, 2985–2993 (2007)
152. V.V. Stolyarov, R. Lapovok, Effect of backpressure on structure and properties of AA5083 alloy processed by ECAP. J. Alloy. Compd. **378**, 233–236 (2004)
153. V.V. Stolyarov, R. Lapovokb, I.G. Brodovac, P.F. Thomsonb, Ultrafine-grained Al-5 wt.% Fe alloy processed by ECAP with backpressure. Mater. Sci. Eng. A **357**, 159–167 (2003)
154. J.Z. Li, W. Xu, X. Wu, H. Ding, K. Xia, Effects of grain size on compressive behaviour in ultrafine grained pure Mg processed by equal channel angular pressing at room temperature. Mater. Sci. Eng. A **528**, 5993–5998 (2011)
155. C. Xu, K. Xia, T.G. Langdon, Processing of a magnesium alloy by equal-channel angular pressing using a back-pressure. Mater. Sci. Eng., A **527**, 205–211 (2009)
156. S. Xiang, K. Matsuki, N. Takatsuji, M. Tokizawa, T. Yokote, J. Kusui, K. Yokoe, Microstructure and mechanical properties of PM 2024Al-3Fe–5Ni alloy consolidated by a new process, equal channel angular pressing. J. Mater. Sci. Lett. **16**, 1725–1727 (1997)
157. R. Lapovok, D. Tomus, C. Bettles, Shear deformation with imposed hydrostatic pressure for enhanced compaction of powder. Scripta Mater. **58**, 898–901 (2008)
158. W. Xu, X. Wu, D. Sadedin, G. Wellwood, K. Xia, Ultrafine-grained titanium of high interstitial contents with a good combination of strength and ductility. Appl. Phys. Lett. **92**, 0119241-3 (2008)
159. T. Sheppard, Extrusion of aluminium alloys. Kluwer Academic Press, Boston USA. Dordrecht. The Netherlands (1999), ISBN 041259070 0
160. P. Loewenstein, L.R. Aronin, A.L. Geary, Powder Metallurgy, in W. Leszyski, (ed.), (Interscience, 1961) pp. 563–583
161. Powder Metal Technologies and Applications was published in 1998 as Volume 7 of ASM Handbook
162. P. Roberts, Technical Paper MF 76-391, SME (1976)
163. R. Casati, A. Fabrizi, A. Tuissi, K. Xia, M. Vedani, ECAP consolidation of Al matrix composites reinforced with in-situ γ-Al_2O_3 nanoparticles. Mater. Sci. Eng. A **648**, 113–122 (2015)